Mechanistic analysis of highly active nitrogen-doped carbon nanotubes for the oxygen reduction reaction

Jorge Vazquez-Arenas*, Drew Higgins, Zhu Chen, Michael Fowler, Zhongwei Chen**

Department of Chemical Engineering, Waterloo Institute for Nanotechnology, Waterloo Institute for Sustainable Energy, University of Waterloo, 200 University Avenue West, Waterloo, ON, Canada N2L 3G1

ABSTRACT

The kinetics of the oxygen reduction reaction (ORR) occurring on nitrogen-doped carbon nanotubes (NCNT) and carbon supported platinum (Pt/C) catalysts in alkaline conditions is analyzed through rotating ring disk electrode (RRDE) measurements and modeled based on typical mechanisms reported in the literature. The purely chemical intermediate reactions are found to be insensitive in the modeling of this mechanism, whereby the models can be simplified to the occurrence of parallel two and four electrochemical electron pathways. Rotating ring disk measurements are shown to be an alternative technique to split the total current density into partial currents that could be associated with the respective reaction pathways. Experimental comparisons of the NCNT and Pt/C catalysts revealed that the ORR kinetics on these materials proceeds similarly throughout two and four electron pathways. The four-electron pathway is found to be the most dominant in both catalysts. Kinetic improvements for the NCNT catalysts are observed, positioning them as promising materials for the ORR catalysis in fuel cells.

© 2012 Elsevier B.V. All rights reserved.

1. Introduction

In recent years, the demand for new materials for low temperature fuel cells applications has increased considerably. This perpetuated interest stems primarily from the limited performance and high system cost of this technology. It is of prime concern to develop electrocatalyst materials with improved oxygen reduction reaction (ORR) kinetics, while simultaneously reducing the excessive cost of the currently utilized carbon supported platinum (Pt/C) metal catalysts. Pt/C has been demonstrated as an excellent material for ORR catalysis; however, the limited natural abundance and steadily increasing cost renders its long term applicability unpractical for commercial purposes. To this concern, non-noble electrocatalysts have been developed as alternatives to Pt-based catalysts either in acidic [1] or alkaline conditions [2–4]. In alkaline conditions, several different types of non-noble catalyst have been explored, including transition metal oxides [3] or alloys [4]; however, their current state of development is not sufficient for application in new age fuel cells. Recently, greatly enhanced ORR activity of CNT has been attained by nitrogen doping, which leads to the formation of nitrogen-doped carbon nanotubes (NCNT). NCNT catalysts with better electrocatalytic activity in alkaline conditions and long-term stability compared to Pt/C have been synthesized [5], with numerous studies elucidating the nature of performance improvements and essential properties of these materials [6–8]. For NCNT, nitrogen on the surface of the CNT is an essential requirement to obtain catalytically active sites.

To date, comprehensive modeling to account for the ORR mechanism occurring on these catalysts has not been addressed. A deeper understanding of the ORR mechanism occurring on NCNT would allow further improvement of the ORR kinetics occurring on these materials. Therefore, this study analyzes the ORR mechanism on highly active NCNT non-noble electrocatalysts formed using ethylenediamine (EDA-NCNT) as a nitrogen and carbon precursor [1,6]. The high ORR activity observed for EDA-NCNT and the additional benefits of using CNT based materials as electrode catalysts due to their superior mechanical properties [9], thermal properties [10], and low cost, positions EDA-NCNT as a potential replacement material to Pt-based catalysts in fuel cell cathodes. Experimental measurements using a rotating ring disk electrode setup are used to evaluate the electrocatalytic activity of these materials along with commercial Pt/C for comparison. Three different physicochemical models accounting for the diffusion, as well as the convection of adsorbed and dissolved species in the boundary layer adjacent to the working electrode are developed to accurately describe the experimental results. These models are based on typical reaction mechanisms reported for ORR in the literature under alkaline conditions. The models are statistically fit to the obtained

* Corresponding author. Tel.: +1 519 888 4567x31622; fax: +1 519 746 4979.
** Corresponding author.
E-mail addresses: jgvazque@uwaterloo.ca, jorge_gva@hotmail.com
(J. Vazquez-Arenas), zhwchen@uwaterloo.ca (Z. Chen).

experimental data in order to estimate the kinetic parameters associated with each model. A sensitivity analysis is performed for the RRDE measurements to discriminate the significance of the reaction mechanisms in the models, and to elucidate the most appropriate mechanism for NCNT catalysis.

2. Experimental

2.1. NCNT synthesis

NCNT synthesis was carried out by a simplistic chemical vapor deposition (CVD) growth method. Ferrocene (98%, Aldrich) as a growth catalyst was dissolved (2.5 wt.%) in ethylenediamine (98% EMD Chemicals) precursor. Small quartz tubes were utilized as the growth substrate and were placed in the center of a larger alumina tube running through the center of a furnace. Synthesis was carried out by heating the tube furnace to 800 °C and injecting the precursor solution under argon protection. Growth was carried out for 1 h, and the final NCNT products were obtained from the inside of the quartz tube substrates. NCNT were washed in 0.5 M sulfuric acid for 5 h and dried in an oven overnight.
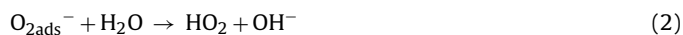
2.2. Oxygen reduction reaction activity evaluation

The electrocatalytic activity towards ORR was evaluated using RRDE voltammetry. Testing was carried out using a bipotentiostat (Pine Instrument Co., AFCBP-1) connected to a rotation speed controller (Pine Instrument Co., AFMSRCE). Experiments were carried out in an alkaline electrolyte using $100 \, mol \, m^{-3}$ KOH. A Pt wire counter electrode and a double junction Ag/AgCl reference electrode were utilized for all testing, and the potentials referred to in this work are on this scale. A glassy carbon electrode surrounded by a Pt ring was used as the working electrode. $20 \, \mu L$ of a catalyst ink solution (4 mg of catalyst dispersed in 2 mL of 0.2 wt.% Nafion solution) was directly applied onto the glassy carbon disk electrode. The working electrode potential was swept from 0.2 to $-1.2 \, V$ vs. Ag/AgCl (figures only to $-0.5 \, V$ vs. Ag/AgCl) at a scan rate of $0.01 \, V \, s^{-1}$. The ring potential was maintained constant at 0.5 V vs. Ag/AgCl. Before testing, the electrolyte was saturated with nitrogen gas and a potential sweep was performed in order to obtain a background reading, which was removed from the subsequently measured currents obtained during ORR testing. After the background scan, oxygen gas was introduced to saturate the solution. The experiments were performed at the same scan rate with different working electrode rotation speeds. A saturated O_2 environment was kept during the experiments, which ensured the collection of reproducible voltammograms.
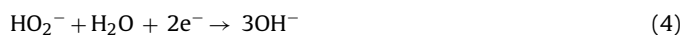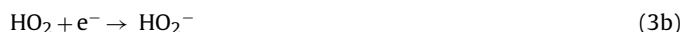
3. Modeling

The models used in the present study consider the kinetics of typical ORR processes occurring on NCNT and Pt/C catalysts. On these surfaces, the ORR mechanism is complicated and could involve several different intermediates. The identity of intermediate compounds depends primarily on the composition of the catalyst and electrolyte. In this section, three physicochemical models are developed considering the kinetics of ORR mechanisms that have been previously proposed [11–16]. In the next section, the models are applied to analyze the RRDE experimental data and evaluate their validity. The first proposed ORR mechanism is based on the study reported by Xu et al. [14] and Appel et al. [15]. In this reaction mechanism, elementary steps are considered for the reduction of oxygen (O_2) and hydroperoxide (HO_2^-) species. In the last reaction of the proposed mechanism, the HO_2^- generated

by two different pathways reacts with water molecules to form hydroxyl ions via a two-electron transfer reaction.

$$O_2 + e^- \rightarrow O_{2ads}^- \tag{1}$$

$$O_{2ads}^- + H_2O \rightarrow HO_2 + OH^- \tag{2}$$

$$HO_2 + O_2^- \rightarrow HO_2^- + O_2 \tag{3a}$$

or

$$HO_2 + e^- \rightarrow HO_2^- \tag{3b}$$

$$HO_2^- + H_2O + 2e^- \rightarrow 3OH^- \tag{4}$$

In the above equations, the subindex ads stands for an adsorbed state of the species, whereas soluble species are specified without a subindex. The second and third models investigated are based on the typical ORR mechanisms involving the straightforward two- and four-electron reduction pathways. The kinetics of model 2 only considers a two-electron pathway where molecular oxygen is reduced to hydrogen peroxide. This intermediate is further reduced to form OH^- [11–13,16].

$$O_2 + H_2O + 2e^- \rightarrow HO_2^- + OH^- \tag{5}$$

$$HO_2^- + H_2O + 2e^- \rightarrow 3OH^- \tag{6}$$

The third model entails the former two-electron pathways (reactions (5) and (6)), in addition to a parallel direct four-electron pathway.

$$O_2 + 2H_2O + 4e^- \rightarrow 4OH^- \tag{7}$$

More detailed ORR mechanisms have been reported in the literature based on several different materials, including NCNT catalysts [13,14,17,18]. Although some of these mechanisms can be very complex [17,18], the characterization techniques used in this work (e.g. voltammetry) are not sensitive to most of these reaction steps. Possible causes of the lack of sensitivity could be the short time domains and life-time of the species generated on the surface of the catalysts. Specifically, their generation-consumption rates are extremely fast compared to the detection limit of the technique. Therefore, only those reaction mechanisms where the detection limit is not entirely restricted have been considered.

3.1. Electrode reaction mechanism and kinetics

The partial current density for electrochemical reactions (1), (3b) and (4)–(7) considering Langmuir adsorption behavior, and without assuming rate-controlling steps are described below. The backward direction of each step is neglected on these expressions.

Reaction (1):

$$\frac{j_1}{F} = k_1 \exp\left(-\alpha_1 \frac{FE'}{RT}\right)(1 - \theta_{O_{2,ads}^-})C_{O_2}^s \tag{8}$$

Reaction (3b):

$$\frac{j_{3b}}{F} = k_{3b} \exp\left(-\alpha_{3b} \frac{FE'}{RT}\right) C_{HO_2}^s \tag{9}$$

Reaction (4):

$$\frac{j_4}{2F} = k_4 \exp\left(-2\alpha_4 \frac{FE'}{RT}\right) C_{HO_2^-}^s \tag{10}$$

Reaction (5):

$$\frac{j_5}{2F} = k_5 \exp\left(-2\alpha_5 \frac{FE'}{RT}\right) C_{O_2}^s \tag{11}$$

Reaction (6):

$$\frac{j_6}{2F} = k_6 \exp\left(-2\alpha_6 \frac{FE'}{RT}\right) C_{HO_2^-}^s \tag{12}$$

Reaction (7):

$$\frac{j_7}{4F} = k_7 \exp\left(-4\alpha_7 \frac{FE'}{RT}\right) C_{O_2}^s \tag{13}$$

where $C_{O_2}^s$, $C_{HO_2}^s$ and $C_{HO_2^-}^s$ represent the surface concentrations of O_2, HO_2 and HO_2^-, respectively, while $\theta_{O_2,ads}^-$ is the fraction of the electrode area covered by $O_{2,ads}^-$. Moreover, k_x and α_x are the rate constant and charge transfer coefficient, respectively for reaction x and E' is the electrode potential corrected for the electrolyte ohmic resistance R_s, i.e.,

$$E' = E - jR_s \tag{14}$$

In voltammetry, the potential E is varied linearly with time at a known rate, i.e.,

$$E = E_{ini} - s_{rate}t \tag{15}$$

where E_{ini} is the starting potential (V) and s_{rate} is the scan rate (V s^{-1}).

The faradaic current density for model 1 is given by the following equation:

$$j_{M1} = j_1 + j_{3b} + j_4 \tag{16}$$

Model 2 involves reactions (5) and (6). Thus, the faradaic current density for this model yields:

$$j_{M2} = j_5 + j_6 \tag{17}$$

Additionally to reactions (5) and (6), model 3 entails a direct four electron pathway (reaction (7)). The faradaic current density of this model can be defined as:

$$j_{M3} = j_5 + j_6 + j_7 \tag{18}$$

The total current density measured during the potential scan is only composed of faradaic (j_{My}) since the capacitive component has been removed from the experimental measurements (e.g. background reading):

$$j_T^y = j_{My} \tag{19}$$

where y is the number of the model.

The material balance for the sites on the catalyst surface occupied by adsorbed species (e.g. $O_{2,ads}^-$) is described below.

$$\Gamma_{O_2,ads^-} \frac{d\theta_{O_2,ads^-}}{dt} = k_1 \exp\left(-\alpha_1 \frac{FE'}{RT}\right)(1 - \theta_{O_2,ads^-})C_{O_2}^s - k_2\theta_{O_2,ads^-} \tag{20}$$

where Γ_{O_2,ads^-} represents its adsorption density required to completely fill a monolayer.

3.2. Transport model development

The following assumptions are made to develop the transient kinetic-transport equations applicable to a rotating ring disk working electrode:

(a) The current distribution is uniform over the RRDE; only transport in the y-direction normal to the electrode surface is considered.
(b) The transport and kinetic parameters are uniform throughout the system.
(c) The solution is isothermal at 298 K.
(d) Ideally dilute behavior is assumed in the solution (i.e. activity coefficients are equal to 1.0).
(e) Since the solution contains a supporting electrolyte, migration of electroactive species is neglected in comparison to diffusional

Table 1
Constants obtained from the fitting procedure of model 1.

Parameter	Value
D_{O_2}	3×10^{-9} m^2 s^{-1}
D_{HO_2}	2.45×10^{-10} m^2 s^{-1}
$D_{HO_2^-}$	2.65×10^{-10} m^2 s^{-1}
υ	1×10^{-6} m^2 s^{-1} [a]
$\Gamma_{HO_2^-}$	1.0×10^{-5} m^2 s^{-1}

[a] Ref. [23].

and convective transport [19]. In addition, O_2 molecules are considered neutral.

The solution is separated into a boundary layer region of thickness δ and a well-mixed bulk region where concentrations are uniform. The bulk region is considered to be fully established at a distance of 3δ from the electrode [20,21]:

$$\delta = 1.61 D_i^{1/3} \Omega^{-1/2} \upsilon^{1/6} \tag{21}$$

where D_i is the diffusion coefficient of any species involved in a transport-controlled reaction, Ω is the rotational speed of the working electrode and υ is the kinematic viscosity of the solution (see Table 1 for numerical values used in this study).

The one-dimensional diffusional and convective flux $N_i(y, t)$ of the dissolved species i (e.g. O_2, HO_2^-) can be expressed as:

$$N_i = -D_i \frac{\partial C_j}{\partial y} + \upsilon_y C_i \tag{22}$$

where

$$\upsilon_y = -0.51023 \Omega^{3/2} \upsilon^{-1/2} y^2 \tag{23}$$

The transient mass balances for O_2 and HO_2^- species within the boundary layer region $0 < y < 3\delta$ are:

$$\frac{\partial C_i}{\partial t} = -\nabla \cdot N_i \tag{24}$$

The concentration of each species at $y = 3\delta$ is at its bulk level C_i^b, i.e.,

$$C_i(3\delta, t) = C_i^b \tag{25}$$

The boundary conditions at the electrode surface $y = 0$ are given below depending on the model:

Model 1:

$$D_{O_2} \frac{\partial C_{O_2}}{\partial y}\bigg|_{y=0} = \frac{j_1}{F} - k_{3a}C_{HO_2}^s \tag{26}$$

$$D_{HO_2} \frac{\partial C_{HO_2}}{\partial y}\bigg|_{y=0} = -k_2\theta_{O_2,ads^-} + k_{3a}C_{HO_2}^s + \frac{j_{3b}}{F} \tag{27}$$

$$D_{HO_2^-} \frac{\partial C_{HO_2^-}}{\partial y}\bigg|_{y=0} = -k_{3a}C_{HO_2}^s - \frac{j_{3b}}{F} + \frac{j_4}{2F} \tag{28}$$

Model 2:

$$D_{O_2} \frac{\partial C_{O_2}}{\partial y}\bigg|_{y=0} = \frac{j_5}{2F} \tag{29}$$

$$D_{HO_2^-} \frac{\partial C_{HO_2^-}}{\partial y}\bigg|_{y=0} = -\frac{j_5}{2F} + \frac{j_6}{2F} \tag{30}$$

Model 3:

$$D_{O_2} \frac{\partial C_{O_2}}{\partial y}\bigg|_{y=0} = \frac{j_5}{2F} + \frac{j_7}{4F} \tag{31}$$

$$D_{HO_2^-} \left. \frac{\partial C_{HO_2^-}}{\partial y} \right|_{y=0} = -\frac{j_5}{2F} + \frac{j_6}{2F} \tag{32}$$

The model is completed by specifying that the concentration of each species is initially uniform everywhere at its bulk level C_i^b, i.e.,

$$C_i(y, 0) = C_i^b \tag{33}$$

while the surface coverage of $O_{2,ads}^-$ is zero on the surface of the catalyst, i.e.,

$$\theta_{O_{2,ads}^-}(0) = 0 \tag{34}$$

3.3. Numerical solution of model equations and parameter estimation

Numerical values for the various model parameters are estimated by statistically fitting the model to the experimental data. This involves the combination of standard methods for parameter estimation with numerical solution of the model equations presented in the previous sections. The system of PDEs given for each model has been solved using the finite element method in the COMSOL Multiphysics™ 4.1 software package. A second-order Lagrange quadratic polynomial is used as the shape function. An interactive-smart mesh is used to discretize the domain.

The model is statistically fit to the experimental RRDE data to estimate model parameters by minimizing the sum-of-squares error between the model predictions and data. The fitness function (35) based on simplex search and genetic algorithms provided by the MATLAB R2011a toolbox was used [22]:

$$\text{Fitness function} = \sum \left(j_T^y - j_T^{exp} \right)^2 \tag{35}$$

where j_T^y and j_T^{exp} are the model-predicted and experimental total current densities, respectively, obtained at each electrode potential considered along a scan. An Intel Core i7 CPU running at 2.80 GHz with a RAM memory of 8.00 GB was used to carry out the calculations.

4. Model fitting and discussion

A 3-fold methodology was adopted in this work in order to analyze the influence of different reaction steps in the overall mechanism throughout sensitivity analysis. The first step was to fit the experimental data obtained for the NCNT catalysts, and determine the kinetic parameters accounting for the ORR mechanism. As mentioned previously, electrochemical techniques including linear sweep voltammetry are not sensitive enough to consider some reactions due to the short time domains and life-times of several species generated on the surface of the catalysts. Reactions with time durations longer than the discrete detection limit were determined in the second step. Finally the ORR reaction mechanism was simplified by considering only the elementary reactions sensitive to the experimental measurements. This procedure is detailed below.

4.1. Analysis of rotating disk electrode measurements using models 1 and 2

Fig. 1 shows the RRDE voltammetry used to evaluate the electrocatalytic activity of the ORR on NCNT catalysts. These voltammograms were obtained at different working electrode rotation speeds (100, 400, 900 and 1600 RPM) in 100 mol m^{-3} KOH with oxygen saturation maintained at 1 mol m^{-3} by continuous bubbling [24]. A sweep rate of 0.01 V s^{-1} was used to scan the potential from 0.2 V vs. Ag/AgCl in the negative direction. The low overpotential region of these voltammograms is characterized by an
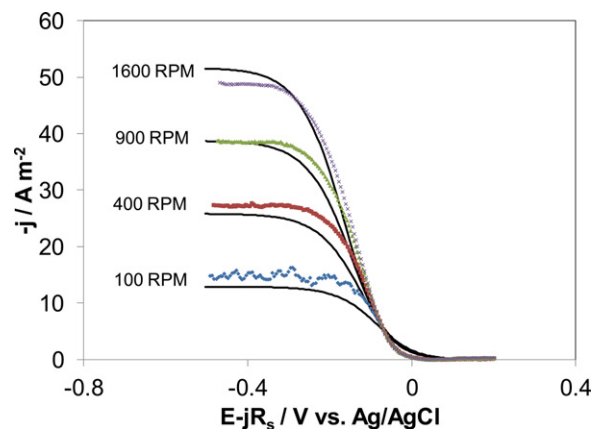
Fig. 1. Model-fitted (black continuous line) and experimental (symbols) linear voltammograms measured at 0.01 V s^{-1} and different rotation speeds on glassy carbon electrodes coated with nitrogen-doped carbon nanotubes. A solution of 100 mol m^{-3} KOH was used as supporting electrolyte. Fits correspond to model 1. Experimental data reprinted with permission from Ref. [2]. Copyright 2009 American Chemical Society.

independence of the current density on the rotation imposed to the electrode, remarking the kinetic control of ORR. A gradual increase of the current density and dependence of rotation is observed to begin at about −0.1 V, suggesting the onset of the mixed control. At more negative potentials, a limiting current density is attained for all rotations, denoting the mass-transport control of the ORR. At −0.1 V, the total number of electrons calculated for the NCNT and Pt/C catalysts were 3.63 and 3.55, respectively. This implies that the ORR on these surfaces entails more than 3 electrons, indicating that more than two reactions might be implicit.

Continuous lines in Fig. 1 indicate the computed polarization curves obtained by the fit process at different rotation rates. A good agreement is observed between the experiments and the model predictions. Slight deviations are obtained for the mixed region, which could be associated with additional contributions not considered by the model, e.g. specific adsorption of ions [16] and heterogeneities of the catalyst. The constants and kinetic parameters obtained from this procedure are reported in Tables 1 and 2, respectively. It is worth mentioning that an effort was carried out to get these constants from literature with limited success. Therefore, they were incorporated in the fitting sub-routine along with the kinetic parameters. It was found that the diffusion coefficients and the maximum adsorption density (refer to Table 1) are in the range of typical diffusion coefficients reported for other species with similar atomic size [20,21,23].

A sensitivity analysis was performed to determine the significance of the reactions steps involved in the ORR mechanism of model 1. The fit of the model is very sensitive to some parameters and insensitive to others. To more closely assess the certainty of these estimates, simulations were performed by decreasing one parameter by 10% while keeping all others fixed at the values

Table 2
Parameters obtained from the fit of model 1 to the experimental data obtained on NCNT catalysts.

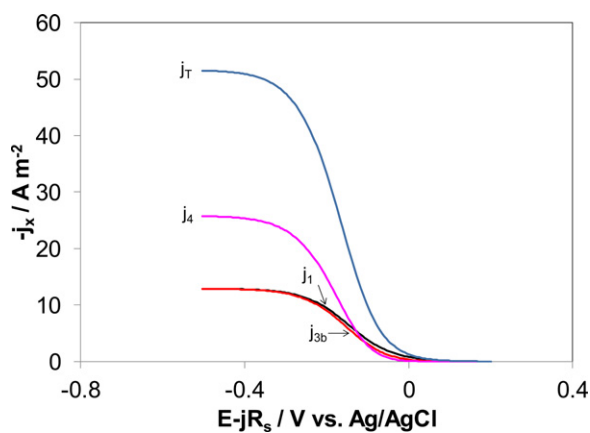| Parameter	Value
α_1	0.47
α_4	0.42
α_5	0.21
k_1	5.85×10^{-5} m s^{-1}
k_2	10 m^2 s^{-1}
k_3	8×10^{-11} m s^{-1}
k_4	4.91×10^{-5} m s^{-1}
k_5	1×10^{-5} m s^{-1}

Fig. 2. Computed partial and total current densities for the electrochemical reactions considered in model 1.

Fig. 3. Variation of surface O_2 and HO_2^- concentration during the potential scans operated at $0.01\ V\ s^{-1}$ and two different rotations (100 and 1600 RPM). The calculations were carried out using model 2 and the parameters shown in Table 3.

obtained from the initial model fitting. The sensitivity of the electrode response to changes in variables or parameters associated with a particular step of a reaction mechanism also reflects the extent to which the overall reaction rate is controlled by that step. The electrode response is sensitive to changes in variables or parameters associated with the rate-controlling step. Conversely, if a step does not control the rate, then the electrode response will be insensitive to changes associated with it. The results of this analysis were very straightforward – only those reaction steps involving charge transfer are sensitive to the model, whereas the chemical reaction (2) between superoxide ($O_{2,ads}^-$) and water, as well as the regeneration of oxygen (3a) has fast kinetic rates beyond the detection limit of electrochemical measurements. The polarization curves in Fig. 2 reflect this conclusion where the total current density can be split into three electrochemical reactions. According to this figure, two electrons are transferred in the first two electrochemical steps (reactions (1) and (3b)), followed by the reduction of hydroperoxide species (HO_2^-) which involves the transfer of two additional electrons (reaction (4)). Thus, as considered in other studies [11–13], the reaction mechanism can be simplified to two electrochemical steps each involving two-electron transfer (i.e. model 2).

Similar fitting procedures were applied for model 2. Fitting model 2 to the experimental data recorded for NCNT catalysts yielded similar results compared to Fig. 1, and therefore, they are not shown herein. The kinetic parameters accounting for the ORR mechanism are detailed in Table 3. As expected, the diffusion coefficients of O_2 and HO_2^- species are similar to those found by model 1 (refer to Table 1). The sensitivity analysis carried out with the kinetic parameters of model 2 revealed that reactions (5) and (6) are sensitive to the model, and this reaction mechanism accounts accurately for the ORR.

Further insight into the system was provided through the computation of non-measured variables (e.g. surface concentrations). Fig. 3 shows the effects of two different rotations (100 and 1600 RPM) on the surface concentrations (C_x^s) of O_2 and HO_2^- species. According to this figure, $C_{O_2}^s$ starts to decay at more positive
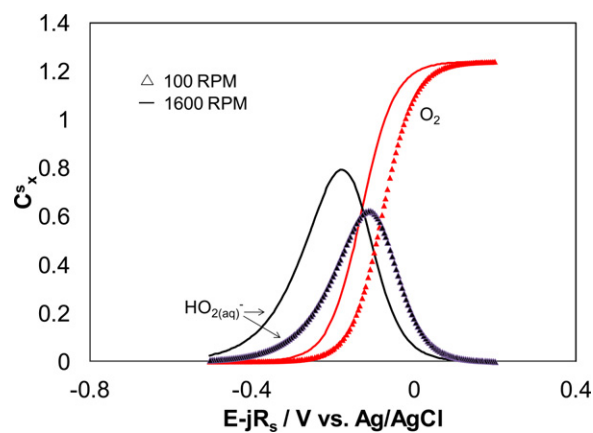
Table 3
Parameters obtained from the fit of model 2 to the experimental data obtained on NCNT catalysts.

Parameter	Value
α_6	0.32
α_7	0.18
k_6	$4.55 \times 10^{-5}\ m\ s^{-1}$
k_7	$3.34 \times 10^{-9}\ m\ s^{-1}$

potentials when the rotation applied to the electrode is lower. This effect is not surprising considering that lower rotations lead to limited convective inputs of O_2 to the surface of the catalyst. Thus, the depletion of O_2 occurs earlier for the experiment carried out at 100 RPM. This can be observed in Fig. 3 at potentials of ca. $-0.25\ V$, and $-0.35\ V$ for this rotation value. These potential values are located where the input of mass-transport control is observed (see Fig. 1). The surface concentrations of HO_2^- species are also shown in Fig. 3. These concentration profiles closely follow the surface concentrations of O_2. As O_2 reduction commences, $C_{HO_2^-}^s$ is produced at a constant rate until the reduction of O_2 becomes mass-transport controlled. At this point, a decline in $C_{HO_2^-}^s$ occurs until it approaches to zero at more negative potentials. Once the depletion of HO_2^- species begins, the reduction of O_2 and HO_2^- proceed at different rates evidenced by the lower O_2 concentration profile throughout this region. This phenomenon suggests that the incomplete reduction of oxygen (reaction (5)) proceeds at a faster rate compared to the reduction of the hydroperoxide (reaction (6)). Therefore, HO_2^- species are not consumed as fast as they are produced.

4.2. Hydroxide selectivity ORR mechanism on NCNT catalysts

In the previous section, two different models were analyzed to determine the sensitivity of the reactions in the ORR mechanism. It was determined that the linear sweep voltammetry technique is sensitive enough to measure accurately the two electron pathway proposed in the literature [10–13]. However, an important question arising at this point is whether parallel steps in the ORR mechanism could occur and contribute to oxygen reduction.

Hydroxide selectivity in alkaline electrolytes is an indicator of the efficiency of the catalysts, whereby it provides insight regarding the reduction mechanisms the molecular oxygen during the electrochemical reaction [16]. Hydroxide selectivity is anomalous to H_2O selectivity in acidic electrolytes and can be calculated using the following equation:

$$S_{OH^-} = \left(\frac{j_D - (j_R/N)}{j_D + (j_R/N)} \right) \times 100 \tag{36}$$

where j_D, j_R and N are the disk current density, ring current density and collection coefficient number (0.26). As proposed by Yeager et al., ORR can occur through a four electron pathway where molecular oxygen is reduced to form OH^- (reaction (7)) or, a two electron pathway where molecular oxygen is reduced to hydrogen
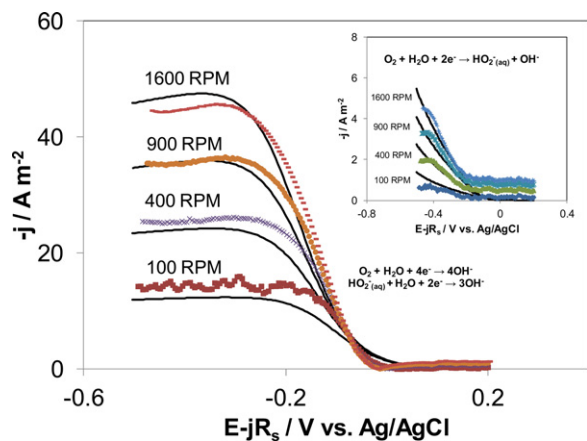
Fig. 4. Model-fitted (black continuous line) and experimental (symbols) linear voltammograms measured at 0.01 V s^{-1} and different rotation speeds on glassy carbon electrodes coated with nitrogen-doped carbon nanotubes (main plot) and a Pt ring (inset). A solution of 100 mol m^{-3} KOH was used as supporting electrolyte. Fits correspond to model 3 (refer to Table 4).

Experimental data reprinted with permission from Ref. [2]. Copyright 2009 American Chemical Society.

peroxide (reaction (5)), which further reduces to form OH$^-$ (reaction (6)) [12,13].

To assess the simultaneous occurrence of these parallel reactions, we conducted rotating ring disk electrode experiments by applying a reductive potential in the disk and an oxidative potential in the ring. The intention of these measurements was to identify and quantify the soluble species generated from ORR on the disk by the anodic ring electrode. The oxidative flux of species on the ring can be associated with the hydroperoxide produced from ORR (reaction (5)) that is not further reduced on the surface of the electrocatalyst (reaction (6)) and is released into the electrolyte. Consequently, the current density of the disk involves the current associated with reactions (5)–(7) occurring on the electrocatalyst materials.

Fig. 4 shows two different sets of linear sweep voltammograms where the currents of the disk and the ring have been separated into contributions of reaction (5) (inset of the plot) and reactions (6) and (7) (main plot). The voltammograms were obtained at different rotations (100, 400, 900 and 1600 RPM) of the electrode in the electrolyte solution containing 100 mol m^{-3} KOH and 1 mol m^{-3} O$_2$. A sweep rate of 0.01 V s^{-1} was used to scan the potential from the OCP in the negative direction. A comparison of the current densities displayed in the main plots and those shown in the inset demonstrates that oxygen is mainly reduced through the 4 electron pathway. Experimental evidence of this finding has been previously reported in literature [2,16]. The effects of mass-transport control are also observed in Fig. 4 for both reaction pathways (reactions (5) and (7)). At high overpotential, a plateau in current density is attained as a result of the oxygen depletion on the surface of the disk electrode. This effect also impacts the oxidative current of the ring since the oxidation of HO$_2^-$ depends on its diffusion subsequent to oxygen reduction. Fig. 4 demonstrates the fitting of the experimental data by model 3 (continuous lines). In order to perform this task, the fitness function used for models 1 and 2 had to be modified to account for the partial current densities from the parallel reactions:

$$\text{Fitness function} = \sum \left(j_5^{\text{model 3}} + j_7^{\text{model 3}} - j_5^{\text{exp}} - j_7^{\text{exp}} \right)^2$$
$$+ \sum \left(j_6^{\text{model 3}} - j_6^{\text{exp}} \right)^2 \tag{37}$$

The model predictions shown in Fig. 4 are good considering that a single set of parameters account for different experiments
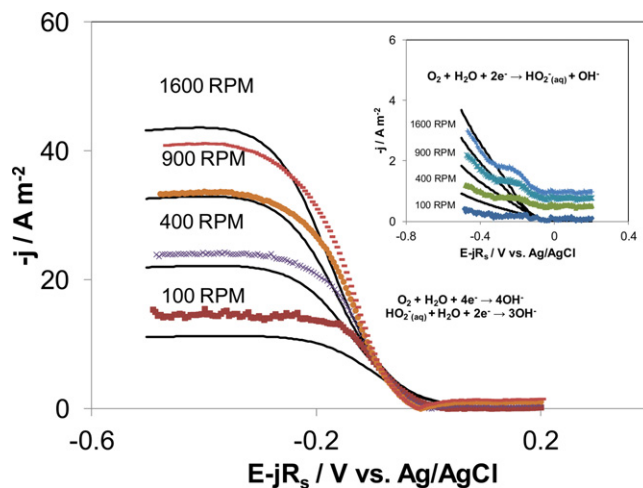
Table 4
Parameters obtained from the fit of model 3 to the experimental data obtained on NCNT catalysts.

Parameter	Value
α_1	0.13
α_4	0.32
α_5	0.14
k_1	5×10^{-6} m s^{-1}
k_2	1×10^{-7} m s^{-1}
k_3	2.31×10^{-7} m s^{-1}

obtained under different conditions. In addition, the heterogeneity (i.e. anisotropy) of these materials is an important effect not considered by the model. The most significant deviation of the model is the prediction of the current plateau related with reaction (6) (refer to the inset of Fig. 4). This deviation is not surprising since that current density is calculated indirectly using an oxidation current rather than a reduction current. Therefore, the model is not capable of identifying those intermediate contributions, which HO$_2^-$ species overcome before being oxidized on the ring, e.g. diffusion and convection from disk to ring. However, these inputs are well described before mass-transfer control is reached. The kinetic parameters obtained from the fitting procedure are reported in Table 4. It was found that the diffusion coefficients (D_{O_2} and D_{HO_2}) did not vary with respect to those shown in Table 1 for models 1 and 2 (e.g. these parameters rely on the mass-transport control region). However, the kinetic parameters obtained with models 1 and 2 present significant changes, whereby rotating ring disk measurements are needed to describe properly the ORR mechanism of NCNT catalysts.

4.3. Hydroxide selectivity ORR mechanism on Pt-catalysts

For conventional carbon electrodes in acidic and alkaline conditions, it has been reported that the ORR generally follows the two electron pathway (e.g. reactions (5) and (6)) [20]. In order to explore this occurrence, ORR was conducted onto commercial Pt/C catalysts, and thus, its kinetics was compared to that of the NCNT catalysts. Fig. 5 shows experiments carried out on commercial Pt/C surfaces. As observed from the comparison between Figs. 4 and 5, the current densities associated with the reduction processes are higher on the NCNT catalysts than on Pt/C. These differences are not

Fig. 5. Model-fitted (black continuous line) and experimental (symbols) linear voltammograms measured at 0.01 V s^{-1} and different rotation speeds on commercial Pt-catalysts (main plot) and a Pt ring (inset). A solution of 100 mol m^{-3} KOH was used as supporting electrolyte. Fits correspond to model 3 (refer to Table 5).

Experimental data reprinted with permission from Ref. [2]. Copyright 2009 American Chemical Society.

Table 5
Parameters obtained from the fit of model 3 to the experimental data obtained on Pt-C catalysts.

Parameter	Value
α_1	0.13
α_4	0.30
α_5	0.13
k_1	3.3×10^{-6} m s^{-1}
k_2	8.6×10^{-8} m s^{-1}
k_3	3.9×10^{-7} m s^{-1}

significant but they emphasize the potential application of NCNT to replace Pt/C catalysts in fuel cells. The qualitative similarities presented between these catalysts might suggest a similar ORR kinetic on these materials. The existence of a low current density on the ring (see inset in Fig. 5) confirms this, and justifies the use of model 3 to account for the experimental data shown in Fig. 5. In other words, the ORR mechanism on Pt/C surfaces also proceeds through 4 and 2 electron pathways (reactions (5)–(7)). Table 5 reveals that there are not significant variations with the kinetic parameters found for the NCNT catalysts (Table 4). However, as observed in Figs. 4 and 5, the current density associated with the two and four-electron pathways for the ORR mechanism are slightly higher onto the NCNT catalysts (see Fig. 4) with a direct comparison provided in a previous report [2]. Not surprisingly, this higher activity is related to the higher kinetic parameters (rate constants and transfer coefficients) obtained on NCNT (Table 4). Thus, on this material the rate constants of the two-electron pathway are higher, as well as the transfer coefficient for the four-electron pathway.

5. Conclusions

ORR kinetics occurring on NCNT and Pt/C catalysts were analyzed through typical mechanisms reported in literature. It was found that not all reactions involved in the reaction mechanisms are sensitive to the current density response. Particularly, those steps involving chemical reactions were found to be insensitive in the model, as a result of their rapid occurrence. On the other hand, linear sweep voltammetry was sensitive to two and four electron pathways for ORR. The kinetic parameters obtained from fitting the models to experimental data strongly depend on the reactions proposed in the mechanism. Thus, the insensitivity of some reaction steps in the model and the excess of degrees of freedom between the experiments and the model predictions can lead to misestimate the kinetic parameters. Rotating ring disk measurements showed to be an alternative technique to split the total current density into partial currents that could be associated with the respective reaction pathways. Thus, the determination of the kinetic parameters of the ORR mechanism was improved by reducing the number of degrees of freedom. The sensitivity analysis conducted to evaluate the validity of the different ORR mechanisms analyzed in this work showed that the chemical reaction between superoxide and water, as well as the regeneration of oxygen in the first model presented

fast kinetic rates beyond the detection limit of electrochemical measurements. Thus, the kinetics of the ORR reaction mechanism was simplified to two (model 2) and three (model 3) electrochemical steps. Both models considered a two-electron pathway where molecular oxygen is reduced to hydrogen peroxide, whereas model 3 additionally entailed a parallel direct four-electron pathway. Although it was determined that the ORR mechanism on NCNT and Pt-catalysts was sensitive to the two-electron pathway considered in model 2, a comparison of NCNT and Pt/C catalysts revealed that the ORR kinetics on these materials proceeded via both two and four electron pathways in parallel as described in model 3. The four-electron pathway was found to be the most dominant and model 3 the most suitable ORR mechanism occurring on these catalysts. A slight kinetic improvement onto the NCNT catalysts was observed based on half-cell electrochemical testing and by determination of the ORR kinetic parameters on these materials, rendering NCNT as promising materials for the ORR catalysis in fuel cell technology.

References

[1] Z. Chen, D. Higgins, A. Yu, L. Zhang, J. Zhang, Energy Environ. Sci. 4 (2011) 3167–3192.
[2] Z. Chen, D. Higgins, H. Tao, R.S. Hsu, Z. Chen, J. Phys. Chem. C 113 (2009) 21008–21013.
[3] J. Lee, G.S. Park, H.I. Lee, S.T. Kim, R. Cao, M. Liu, J. Cho, Nano Lett. 11 (2011) 5362–5366.
[4] Q. He, X. Yang, X. Ren, B.E. Koel, N. Ramaswamy, S. Mukerjee, R. Kostecki, J. Power Sources 196 (2011) 7404–7410.
[5] K.P. Gong, F. Du, Z.H. Xia, M. Durstock, L.M. Dai, Science 323 (2009) 760–764.
[6] D. Higgins, Z. Chen, Z. Chen, Electrochim. Acta 56 (2011) 1570–1575.
[7] Z. Chen, D. Higgins, Z. Chen, Electrochim. Acta 55 (2010) 4799–4804.
[8] D. Higgins, J. Wu, W. Li, Z. Chen, Electrochim. Acta 59 (2012) 8–13.
[9] E.W. Wong, P.E. Sheehan, C.M. Lieber, Science 277 (1997) 1971–1975.
[10] S. Berber, Y.K. Kwon, D. Tomanek, Phys. Rev. Lett. 84 (2000) 4613–4616.
[11] A. Damjanovic, M.A. Genshaw, J.O.M. Bockris, J. Chem. Phys. 45 (1966) 4057–4059.
[12] E. Yeager, J. Mol. Catal. 38 (1986) 5–25.
[13] E. Yeager, Electrochim. Acta 29 (1984) 1527–1537.
[14] J. Xu, W.H. Huang, R.L. McCreery, J. Electroanal. Chem. 410 (1996) 235–242.
[15] M. Appel, A.J. Appleby, Electrochim. Acta 23 (1978) 1243–1246.
[16] Z. Chen, D. Higgins, Z. Chen, Carbon 48 (2010) 3057–3065.
[17] S. Maldonado, K.J. Stevenson, J. Phys. Chem. B 109 (2005) 4707–4716.
[18] J.D. Wiggins-Camacho, K.J. Stevenson, J. Phys. Chem. C 115 (2011) 20002–20010.
[19] J. Vazquez-Arenas, Electrochim. Acta 55 (2010) 3550–3559.
[20] J. Vazquez-Arenas, L. Altamirano-Garcia, M. Pritzker, R. Luna-Sanchez, R. Cabrera-Sierra, J. Electrochem. Soc. 158 (2011) D33–D41.
[21] J. Vazquez-Arenas, M. Pritzker, J. Electrochem. Soc. 157 (2010) D283–D294.
[22] http://www.mathworks.com/help/techdoc, last accessed December 2011.
[23] D.R. Lide (Ed.), CRC Handbook of Chemistry and Physics, Taylor & Francis, Boca Raton, 2004.
[24] K. Kinoshita, Electrochemical Oxygen Technology, in: The Electrochemical Society Series, John Wiley & Son, Inc., 1992.